Preliminary Study and Numerical Investigation of an Electrostatic Unit for the Removal of Fluoride From Thermal Water of Ethiopian Rift Valley

Matteo Bruno Lodi, *Student Member, IEEE*, Fabio Fanari, Alessandro Fanti, *Member, IEEE*, Francesco Desogus, Worash Getaneh, Giuseppe Mazzarella, *Senior Member, IEEE*, and Paolo Valera

***Abstract*—This article deals with the numerical modeling of the multiphysics investigation of an electric-field-based device for the defluoridation of Ethiopian water to mitigate fluorosis while satisfying the World Health Organization quality requirement for potable water. A tubular reactor with metallic parallel plates, connected to a static voltage source, exerts an electric force on the ion in solution, attracting it to the electrodes. Meanwhile, the ion is drifted by the laminar water flow which, in turn, allows us to separate and collect the F^--rich stream from the potable one. In this system, the electrostatic problem and the mass transport are coupled according to the highly nonlinear modified Poisson–Nernst–Planck–Stokes equations system. Therefore, carefully modeling the dielectric permittivity, the ionic diffusivity, and mobility as function of fluoride concentration and temperature, the set of operating parameters to ensure the highest fluoride removal from Ethiopian thermal water is identified.**

***Index Terms*—Electric field, Ethiopia, fluoride removal, Poisson–Nernst–Planck–Stokes model, potable water, thermal water.**

I. Introduction

WATER is a cheap and valuable resource. It must be managed carefully to avoid shortages and prevent the pollution of available sources [1]. Water can be polluted by human or natural causes, such as the presence of trace elements [2]–[6]. If high concentration of naturally occurring fluoride ion (F^-) is found in drinking water sources, then a noticeable increase in the daily load of fluoride can expose the populations to the risk of endemic fluorosis [7]. Fluorine is an abundant trace element and it can be found in rocks and sediments, such as syenites, granites, and alkaline volcanics, in the form of fluorite (CaF_2), micas, biotite, and villiaumite (NaF) [3]. It can be released into groundwaters from rocks and can be particular abundant in water derived from hydrogeothermal sources (the so called "juvenile" water). In many countries around the world, the safety of potable waters affects the population's quotidian lives, as well as their economic development [3], [4]. Most of the areas affected by this problem suffer from scarce water availability [8].

TABLE I
Health Effects Related to the Different Fluoride Concentration in Drinkable Water [9], [12]

F^- Concentration ($mg{\cdot}l^{-1}$)	Effects on Human Health
< 0.5	Tooth decay
0.5 - 1.5	Optimal Dental Health
1.5 - 4	Dental Fluorosis
4 - 10	Skeletal Fluorosis
> 10	Paralyzing Fluorosis

A major concern is the human health effects of the prolonged exposure to F^-, which can lead to the health outcomes presented in Table I [9]. Above the optimal threshold value of 1.5 $mg{\cdot}L^{-1}$, the fluoride accumulates in the tooth mineral matrix initiating the displacement of hydroxide ions from the hydroxyapatite ($Ca_5(PO_4)_3(OH)$)), forming fluoroapatite, $Ca_5(PO_4)_3F$. This less soluble mineral compound makes bone denser and tougher, and initially it is strengthened. However, as the fluoride intake increases, the bone becomes very brittle, thus leading to dental fluorosis [10]. It has been reported that higher dose of F^- in drinking water (up to 4 $mg{\cdot}L^{-1}$) damages the gastrointestinal system or bring chronic kidney disease [3], [11], [12]. As the exposure to fluoride increases, becoming prolonged and severe, the ion tends to distribute in the whole body promoting cancer occurrence and altering the whole bone tissue homeostasis and metabolism, causing skeletal fluorosis and even death [10] (see Table I).

The health risk derived from fluoride-polluted water is a relevant worldwide issue. In Asia (e.g., China, India, and Pakistan), Africa (e.g., Sudan, Tanzania, Kenya, and Uganda), Turkey, and Mexico [3], the problem has reached an endemic size since several million people are affected by osteodental fluorosis [2], [13]. Among the affected countries, in Ethiopia, especially in the Rift Valley (ERT) area, shown in Fig. 1 [14], the presence of

Manuscript received December 12, 2019; revised March 1, 2020; accepted March 18, 2020. Date of publication April 27, 2020; date of current version June 3, 2020. This work was supported by RAS/FBS under Grant F71/17000190002. *(Corresponding author: Alessandro Fanti.)*

Matteo Bruno Lodi, Alessandro Fanti, and Giuseppe Mazzarella are with the Department of Electrical and Electronic Engineering, University of Cagliari, 09123 Cagliari, Italy (e-mail: matteobrunolodi@ieee.org; alessandro.fanti@diee.unica.it; mazzarella@diee.unica.it).

Fabio Fanari and Francesco Desogus are with the Department of Mechanical, Chemical and Material Engineering, University of Cagliari, 09123 Cagliari, Italy (e-mail: f.fanari@dimcm.unica.it; f.desogus@dimcm.unica.it).

Worash Getaneh is with the School of Earth Sciences, Addis Ababa University, Addis Ababa, Ethiopia (e-mail: worashg@aau.edu.et).

Paolo Valera is with the Department of Civil Engineering and Architecture, University of Cagliari, 09124 Cagliari, Italy, and also with the Institute of Environmental Geology and Geoengineering, National Research Council, 09123 Cagliari, Italy (e-mail: pvalera@unica.it).

This article has supplementary downloadable material available at http://ieeexplore.ieee.org, provided by the authors.

Digital Object Identifier 10.1109/JMMCT.2020.2982766

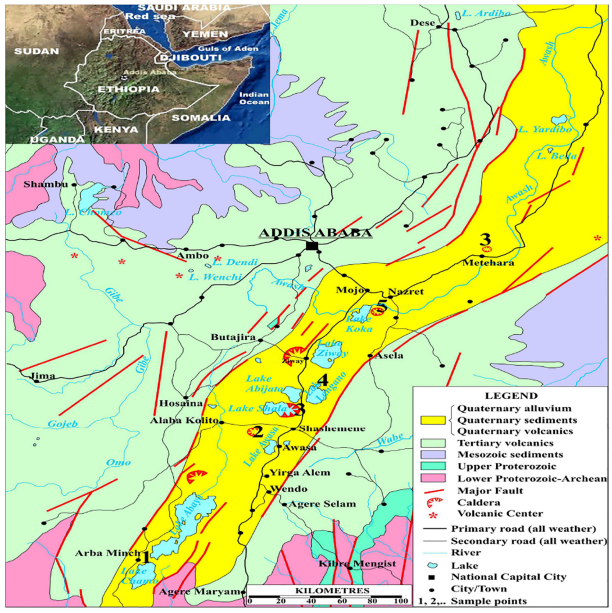

Fig. 1. Geographic and geologic logic map of the Ethiopian Rift Valley area. The sites of interest are highlighted in the map.

wells, lakes, and rivers rich in fluoride is a national problem and the mitigation of such social plague is a serious public health problem [15], [16]. Indeed, in these rural regions, only about 30% of the population has access to safe drinking water [15]. To fight such a serious public health problem, several policy administrations should be worked out to identify the best water saving and fluoride-removal technologies [17].

A common technology for fluoride removal is precipitation, which consists of using aluminum sulphate to create an insoluble salt reacting with the fluoride in the water [3], [18]. Even though this strategy can be implemented at the community level, it has an efficiency of 65–70% and has the drawbacks of requiring the collection of precipitate and also of leaching aluminum in the treated water [13], [15], [16].

Adsorption techniques are often employed to subtract F^- ion from potable waters [19], [20]. A very wide range of adsorbing materials have been investigated in the literature [2], [3], [13], [18], [21]. Calcite, alumina-based composites, zeolites, and others present positive free-charges on their surface can adsorb the free fluoride ions, which diffuse from the bulk of the solution [2]. Despite innovative nanomaterials, the ideal adsorbent would be an efficient, low-cost, and easily accessible material. However, the removal efficiency varies from 50% for some clays to 90% for zeolites. Other limitations of this method are that the pH of the solution must be optimized and that sulphate, phosphate, and bicarbonate can compete, limiting the selectivity [3]. Finally, the regeneration of the material is limited to maximum tens of cycles, and it is sometimes difficult and requires operators with medium technical skills [2], [3].

A major role in defluoridation is played by membrane processes, namely reverse osmosis (RO), nanofiltration, Donnan dialysis, and Memstill technology [3]. These methods allow the highest removal efficiency (95%), with the advantage that color and taste of the treated water are not affected by the treatment. On the other hand, the membranes employed are often subject to biofouling problems, bacterial contaminations, and degradation, thus highly increasing operating costs and requiring an operator with medium to high competences [3], [13].

Since defluoridation can be regarded as the problem to remove a population of charge from water, electric field to enhance the removal of pollutant ions in membrane methods have been explored [3]. Electrodialysis (ED) systems can reach 80–95% and are able to work with high F^- concentration while performing simultaneous desalination [3]. Even if it is more economical than RO and it is perceived positively by public (even in rural areas [17]), such technique has the shortcomings of requiring long, complicated pretreatment steps and of being not specific, not suitable for water with low salinity, while determining a high water loss, energy consumption (1.5–18 V [22], [23]), and capital costs [3], [24], [25]. Among the electrochemical methods, some other interesting membraneless techniques have been proposed. Electrocoagulation (EC) is a promising emerging technology that exploits an electrolytic process to generate, *in situ*, a coagulant by oxidation of a specific anodic material able to interact with the target ions [3]. EC devices demonstrated a high efficiency (∼100%), but require operators with high technical skills. Furthermore, it is not specific since other anions (e.g., sulphate) can interfere during the process. In EC systems, the electrodes must be replaced due to their consumption and the electric power consumed is very high [3] (e.g., current densities of about 4–100 $A \cdot m^{-2}$ would be required [26]). Another highly effective method for defluoridation is electrosorption (ES), which enhances the removal capacity and regeneration of adsorbent by more than 50%, but requiring high operational and maintenance costs [3].

From the analysis of the literature, the precipitation, adsorption, or membrane techniques are associated with lower costs (except for RO), but also with poorer effectiveness in fluoride removal, together with issues, such as the membrane substitution or the adsorbent regeneration [3], [13]. The electrochemical methods, however, despite being more efficient, are not selective, require operators with high technical skills, and mainly have high costs for installation and maintenance, which are not sustainable for developing countries [3], [25]. The goal of this article is to study the feasibility of an electric-field-based methods, which respects the fundamental requirements of a system intended to be used as fluorosis-mitigation solution in the Ethiopian context [3], [13], [17], as follows:

1) the system should not use chemicals, being environmental friendly and benign;
2) the technology should be readily available for implementation, i.e., the system should admit technical feasibility;
3) the system must have high efficiency (80%–100%);
4) the device should be low cost, affordable, reliable, easy to operate and, hence, accessible to rural communities;
5) the system should account for local specific conditions;
6) the device has to allow up-scaling from household to community level.

Through the knowledge of hydrogeologic conditions of ERT area and taking into account the key criteria for an ideal system

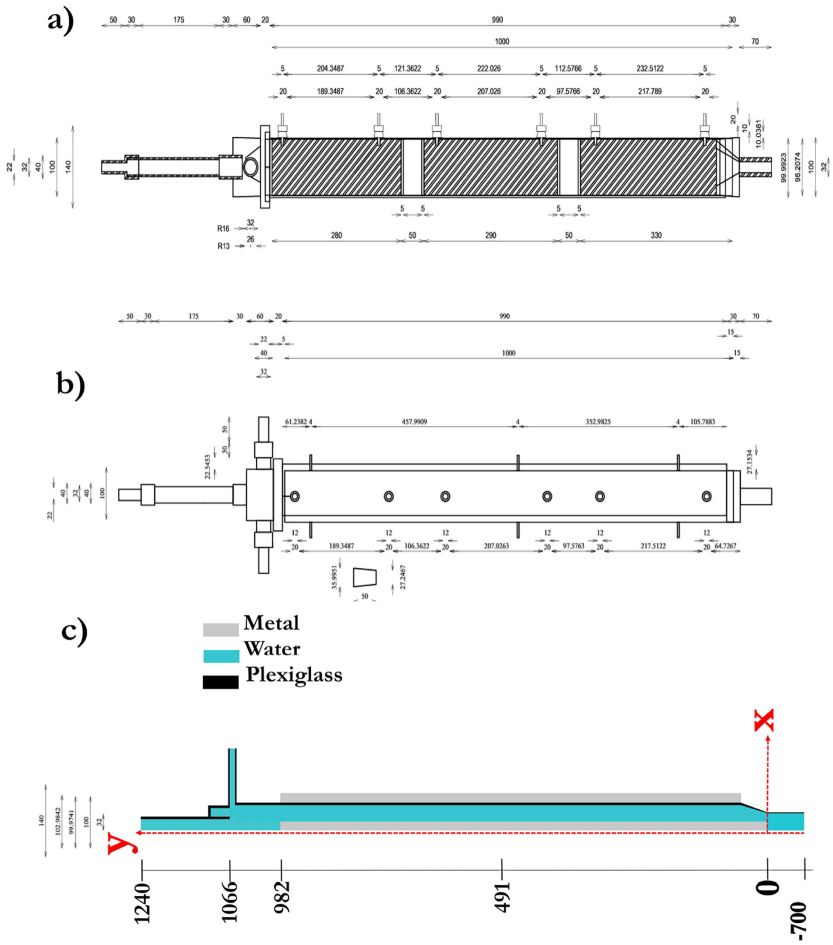

Fig. 2. (a) Lateral view of the prototype of the fluoride removal system. The main tube is removed to highlight the presence of the inner electrode plate. (b) Top view of the defluoridator. The water flows from right to left. (c) Simplified geometry of the prototype for the finite element (FEM) analysis in COMSOL Multiphysics. All dimensions are in millimeters.

for the mitigation of fluorosis, in this work, a preliminary study and an evaluation of technical feasibility are performed to design and investigate an electric defluoridator. The multiphysics nonlinear coupling of the electric and mass transport phenomena are quantitatively, carefully, and critically modeled. In this way, it assessed the functioning of a pilot-scale membraneless electrostatic unit for fluoride removal from F^--rich Ethiopian thermal waters.

II. System Geometry and Functioning

The geometry of the prototype of the electrostatic unit for fluoride removal is presented in Fig. 2. The F^--rich thermal water is conveyed to the reactor through a cylindrical plexiglass pipe with radius r_{in} equal to 1.3 cm. A semiconical transition aperture (70 cm) lets fluoride-rich water to flow in the main body, i.e., a cylinder with radius r_c of 100 mm and 1.1 m in length. A metal plate is positioned at the center of the transverse section and it extends for 1 m along the z-axis of the main body [see Fig. 2(c)] The inner metal plate is not in contact with the bottom of the structure and it is soldered to six pins, which allow the connection to the external voltage generator. The inner electrode is subject to a potential $-\phi_0$. Two bended and curved stainless steel plates are in contact with the outer surface of the main body. These are the external electrodes and are connected to the same voltage, but with opposite sign with respect to the inner electrode, i.e., ϕ_0. The external metal sheets are a set at a distance of 5 cm from the inlet and are 97 cm long, as shown in Fig. 2. In this configuration, considering a salt XF, where X is a monovalent cation, the anions present in the flowing water would be attracted to the lateral surface of the cylinder, whereas the cations would stay nearby the inner electrode plate. With this separation of charges, at the end of the main body, three streams can be recognized: an F^--rich central and two X^+ streams. Therefore, to collect the outlet streams, a three-way outlet is present. With the same dimension of the inlet chamber, this part of the defluoridator tube is necessary to prevent mixing while facilitating the collection of treated and waste water. Analogue considerations hold for the inverse configuration (inner electrode $-\phi_0$—outer electrodes ϕ_0).

The choice of tubular reactors for fluoride removal is frequent in the literature since they allow us to work in a continuous operation mode to increase the volume of treated water per unit time [27]–[29]. The materials required to assemble the

TABLE II
MEAN VALUES OF THE CONCENTRATION OF MOST RELEVANT IONIC SPECIES IN THE FIVE SET OF F^--RICH ETHIOPIAN THERMAL WATER

	Temp. (°C)	F^-, mg·l^{-1}	Cl^-, mg·l^{-1}	Na^+, mg·l^{-1}	Ca^{2+}, mg·l^{-1}	σ, μS·cm^{-1}	pH
Nach Sar	100	9.40	88.9	449	35.4	1910	8.14
Corbetti	100	0.37	5.6	2.8	0.9	72.5	4.3
Shala	96	73.50	1694	2374	0.7	9230	8.8
Langano Est	90	0.277	487.5	793	8.8	3560	7.8
Wongi	50	18.33	26.4	190	3.5	940	8.7
Mean ± Std.		20.369 ± 30.623	460.480 ± 716.888	761.760 ± 948.821	9.860 ± 14.646	3142.500 ± 3640.979	

reactor are steel and plexiglass, which are both easily available in Ethiopia and allow us to construct the device on site, without the need of importing raw materials or complicate manufacturing [17]. The study of this economic defluoridator should be regarded as a valuable alternative to cases where the solutions and technologies discussed in Section I are not feasible or cost-effective for the rural communities.

III. MATERIALS AND METHODS

A. Sampling and Characterization of Ethiopian Waters

The F^--rich waters were collected in five thermal springs from the Ethiopian Rift Valley region, which are shown in Fig. 1.

In each site, after the samples collection, the water was cooled to room temperature and the colorimetric analysis was performed for the nitrates, sulphates, and sulphurs in about 30 min, whereas the carbonates and bicarbonates titration was performed in about 15–20 min. The characterization of Ethiopian waters from Nach Sar, Corbetti, Shala, Langano Est, and Wongi was completed by investigating the pH and their electric conductivity σ.

The values of concentration of ionic species and the microelement analysis on thermal water were quantitatively assessed to employ realistic F^- values in the simulations.

The results of the five samples sites are reported in Table II, from which the chemical variability of the Ethiopian hot springs is evident. It can be noticed that the elemental composition is very different among the sites. This allows us to understand a spectrum of Ethiopian water sources. As regards the fluoride, the samples from Corbetti and Langano East point out a concentration value below the World Health Organization limit. However, the other three sites can be defined as fluoride rich and their measured concentration values agree with the one reported in the work of Tekle-Haimanot *et al.* [30].

B. Model: Modified Poisson–Nernst–Planck–Stokes Equations

In this section, the problem of describing the dynamics and spatial distribution of a z:z symmetric binary electrolyte is introduced and the set of nonlinear coupled equations is presented.

In the literature, the migration dynamic of an ionic population to a charged surface, at which is applied an electrostatic potential ϕ_0, is typically given in terms of the dilute solution theory [31], [32]. Provided that the potential is small enough, under this well-known approximation, the concentration fields are supposed to follow a Boltzmann's distribution

$$C = C_0 e^{\pm ze\phi/k_B T} \tag{1}$$

where z is the ion valence, e is the electron charge, k_B is the Boltzmann constant (J·K^{-1}) and T is the system temperature in K. Anyway, for values of voltage much higher than the thermal voltage ($\phi_t = k_B T/ze$), the ion concentration blows up exponentially and the correspondent spatial charge distribution at the charged surface does not respect the physical limit due to the finite ion size [31], [32]. Therefore, in the literature, several models to modify the Poisson–Boltzmann (PB) equations system have been proposed. To go beyond the naive PB view, the excluded volume effects and the effective charge density distribution were studied using statistical mechanic, but others have focused on ion–ion or ion–wall interactions [31]. Some researchers tackled the problem of the volume effect using molecular dynamic simulations or Monte Carlo simulations [33], [34]. Anyway, the cited solutions are computationally expensive and cannot be easily scaled to any other geometry or at a larger scale. However, for the practical goal of this article, the electromigration problem can be treated relying on modified macroscopic continuum mechanic models [31], [35], [36]. This approach allows us to use nontrivial numerical methods, such as FEM or finite difference, to solve steady-state nonlinear and coupled problems while accounting for the steric and volume effects [31], [37]. In our work, the macroscopic point of view is required to analyze a device that can be used to subtract F^- ions from Ethiopian thermal water rich in F^-, to potentially mitigate the problem of endemic fluorosis. This choice is motivated by a wide literature about the solution existence and the error analysis [37]–[39].

1) Electrostatic Problem: In this article, a z:z symmetric binary electrolyte, with equimolar concentration ($C_0 = C_- = C_+$), is considered. For the sake of representativity of the problem, the binary salt NaF is chosen. Recalling the data derived from the analysis of Ethiopian waters in Table II, the choice is justified since F^- is the target ion and Na^+ is the monovalent ion with the highest concentration for all cases. The numerical framework presented in this article should be able to represent different Ethiopian waters and operating conditions. Since the water–ion composition is very different, the dielectric permittivity of the NaF solutions has been considered as variable with the salt concentrations [41]

$$\epsilon(C) = \epsilon(0) - \delta_\epsilon C + \beta_\epsilon C^{3/2} \tag{2}$$

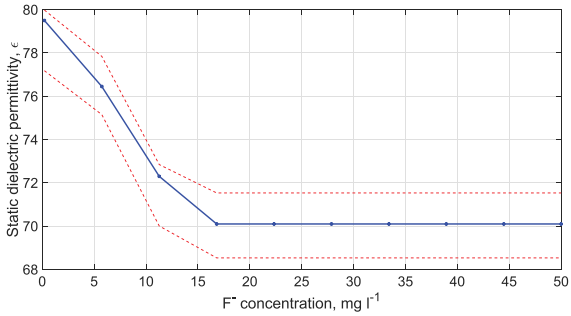

Fig. 3. Variation of the static dielectric permittivity of NaF solution ϵ as a function of fluoride concentration in water. The dashed lines represent the standard deviation of the experimental values from [40].

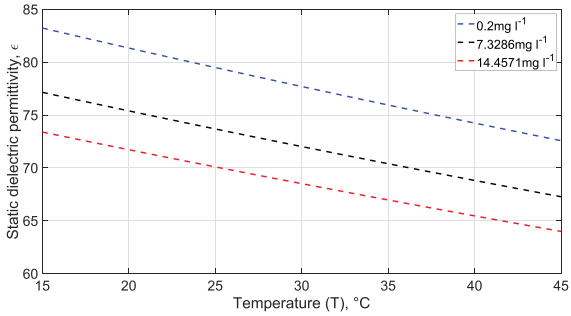

Fig. 4. Dielectric permittivity (ϵ) versus system temperature [42]. The lower the temperature, the higher the dielectric constant. It should be noted that at $T =$ 25 °C, the values of ϵ for a given C_0 equals the value in Fig. 3.

where $\epsilon(0)$ is equal to 78.5 $\pm$ 1.5 and δ_ϵ is equal to 17.8 $\pm$ 1.3 dm^3·mol^{-1} with β_ϵ = 6.0 $\pm$ 1.4 (dm^3·mol^{-1})$^{3/2}$. Equation (2) fits dielectric data at T=25 °C for any given salt concentration of Ethiopian waters in Table II (for further details see Supplementary material). To account for another relevant specific parameter of a spring or water sources in a given location, the temperature dependence of the static dielectric permittivity is assumed to follow the Ray's model [42], [43]

$$\epsilon(T) = \epsilon(C)\left[1 - 4.579 \cdot 10^{-3}(T - T_0) + 1.19 \cdot 10^{-5}(T - T_0)^2 \; - \; 2.8 \cdot 10^{-8}(T - T_0)^3\right] \quad (3)$$

where T_0 is the reference temperature of 25 °C. The variation of ϵ with temperature is shown in Fig. 4 for different fluoride concentrations.

On the other hand, the possible influence of the electric field strength on ϵ is neglected, as motivated in Section SM5 of Supplementary material [44], [45].

The electric potential due to a distribution of charges is evaluated solving the modified PB equation [32]

$$\nabla \cdot (\epsilon \nabla \phi) = zeC_0 \frac{2\sinh\left(\frac{ze\phi}{k_B T}\right)}{1 + 2\nu \sinh\left(\frac{ze\phi}{k_B T}\right)^2} \quad (4)$$

where ϕ is the unknown electrostatic potential in volts, whereas the measure of nondiluteness, which accounts for the steric and volume effects ν, i.e., the mean volume fraction of ions in the bulk, is defined as [31], [32]

$$\nu = 2a^3 C_0. \quad (5)$$

This modification of the model was proved to ensure that the system can saturate to a maximum concentration value equal to $C_{\max} = a^{-3}$. Thus, the amount of charge attracted to the charged surfaces cannot be infinite, avoiding the electrostatic potential to blow up locally, i.e., an effective, but finite, charge density distribution can be found from (4).

2) Nonlinear Electromigration: The macroscopic mass transport balances required to determine the spatio–temporal distribution of the F^- and Na^+ ion in the systems in Fig. 2 are the following nonlinear convection–diffusion equations [32]:

$$\nabla \cdot \left[D\nabla C_\pm \pm ze\mu C_\pm \nabla\phi + \mathbf{v}\nabla C_\pm + a^3 D \frac{C_\pm \nabla(C_+ C_-)}{1 - C_+ a^3 - C_- a^3} \right] = 0 \quad (6)$$

where D is the ion diffusion coefficient in water in m^2·s^{-1} while μ is the ion mobility in m^2·V^{-1}·s^{-1}, and $\mathbf{v}$ is the velocity field in m·s^{-1}.

Both the diffusivity D and mobility μ are considered to be equal for C_- and C_+ ions. These values are generally function of temperature T and the salt concentration [40], [46]. Assuming the system to be in thermal equilibrium, a uniform temperature distribution can be considered during the functioning. Hence, for different water source temperature, the diffusion coefficient will vary proportionally to $k_B T$ according to the Einstein–Stokes formula [46]. The dependence of the concentration of fluoride ions and its counterions is necessary to respect the physical phenomena of saturation of charge attraction to a charged surface and decreased mobility [44], [45]. Considering the ion crowding to a charged surface, i.e., $D, \mu \neq$ const, in the model allows us to evaluate the feasibility of the proposed electrostatic and membraneless defluoridation system. The experimental data of mutual diffusion coefficient from the work of Lu and Leaist [40] are used. A sixth-order polynomial function is used to describe $D(C)$, as shown in Fig. 5 (further details are provided in Section SM6 of Supplementary material). The values used are similar to those reported in [47] and [48]. The ionic mobility is evaluated using the Einstein–Smoluchowski relationship [46], [49]

$$\mu = \frac{D}{\frac{R}{F}T} \quad (7)$$

where R is the universal gas constant in J·mol^{-1}·K^{-1} and F is the Faraday's constant in C·mol^{-1}.

Equation (6) is subject to the Dirichlet boundary condition (BC) at the inlet section of the electrostatic unit

$$C_0 = C_- = C_+. \quad (8)$$

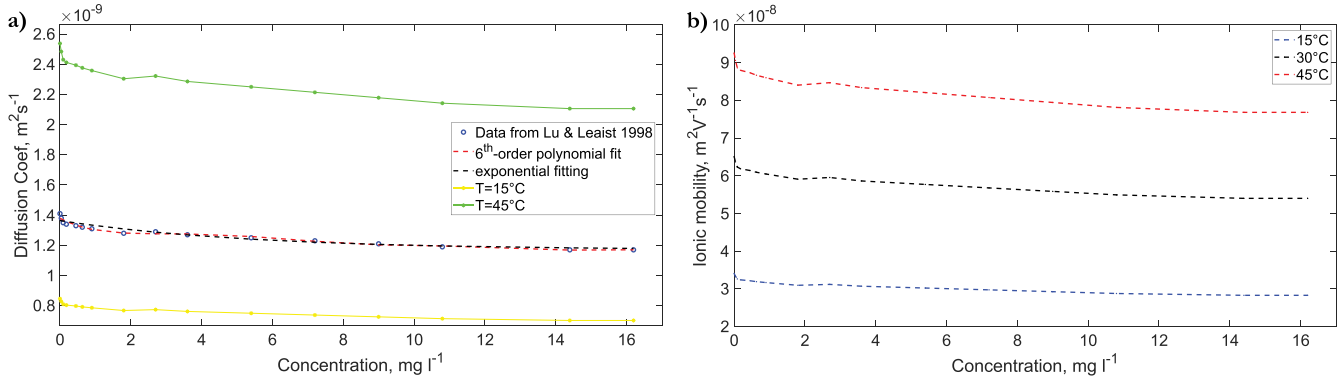

Fig. 5. (a) Mutual diffusion coefficient for NaF solution, in $m^2 \cdot s^{-1}$ at 25 °C [40]. (b) Mutual ionic mobility μ in $m^2 \cdot V^{-1} \cdot s^{-1}$ derived from the experimental data using the Einstein–Smoluchowski relationship. The temperature variation for both physical quantities is shown from 15 to 45 °C.

At the outlet sections and at the wall of the system in Fig. 2 the Neumann BC no-flux BC applies

$$D\nabla C_{\pm} \pm ze\mu C_{\pm}\nabla\phi + \mathbf{v}\nabla C_{\pm} + a^3 D\frac{C_{\pm}\nabla(C_{+}C_{-})}{1 - C_{+}a^3 - C_{-}a^3} = 0. \tag{9}$$

It should be pointed out that in the system no electrochemical reactions can take place at the electrode surface, since two out of three are insulated with plexiglass.

Some important assumptions must be pointed out and discussed to solve the modified Poisson–Nernst–Planck (MPNP) equation [i.e., (6)] properly. First of all, it is assumed that the charging dynamic of the double layer is very fast compared to the residence time of the fluid. Therefore, the mass balance can be solved assuming the system is in steady state. This is verified only if the residence time in the reactor is much larger than the charging time at the electrodes surfaces [32]

$$\tau_{\text{fl}} = \frac{l}{v_0} \gg \tau_{\text{ch}} = \frac{\lambda_D r_{\text{ch}}}{D} \tag{10}$$

where l is the characteristic length of the system in meters, which is chosen to be the length of the defluoridation unit, while v_0 is the initial velocity of the fluid in $m \cdot s^{-1}$ and r_{ch} is the channel radius or, better, the distance between the electrodes plates. The Debye screening length λ_D is defined as [31]

$$\lambda_D = \sqrt{\frac{\epsilon k_B T}{2z^2 e^2 C_0}}. \tag{11}$$

This physical quantity, which is always lower than the characteristic length of the system, i.e., $\lambda_D \ll l, r_{\text{ch}}$, depends on the system temperature and dielectric permittivity of the medium, but inversely from the initial ion concentration, as shown in Fig. S1, Section SM1 and SM2 in Supplementary Material. Ethiopian water sources and spring have temperatures ranging from 15 °C to more than 36 °C, then the Debye length may vary from 76 to 85 nm, for $C_0 = 0.027$ mg·L^{-1}, or can reach a minimum of 4 nm for $C_0 = 73.50$ mg·L^{-1}, if the water composition from the Shala site is considered (see Table II).

The MPNP equation is solved considering that the local bulk conductivity does not change significantly and neglecting the influence of the Bjerrum length[1] and the ion–ion correlations, under a mean field approximation and assuming weekly nonlinear regime [32]

$$2\frac{\lambda_D^2}{a^3 l^2 C_0}\frac{ze\phi_0}{k_B T} \ll 1. \tag{12}$$

With these assumptions, the final goal is to quantify the fluoride removal efficiency at the outlet sections

$$\Gamma = \left.\frac{C - C_0}{C_0}\right|_{\text{Out}} \cdot 100. \tag{13}$$

3) Fluidodynamic Modeling: For a complete mathematical description of the working and performance of the defluoridator system, the velocity field $\mathbf{v}$ of the drift-diffusion equation (6) should be defined [35]. As previously described in Section II, the F^--rich thermal water is allowed to flow from the inlet to the outlet of the unit represented in Fig. 2. Hence, the velocity pattern can be computed according to the Navier–Stokes equation [35], [39], [49]

$$\rho\left(\frac{\partial \mathbf{v}}{\partial t} + \mathbf{v}\cdot\nabla\mathbf{v}\right) = -\nabla P + \eta\nabla^2\mathbf{v} \tag{14}$$

where ρ is the fluid density in kg·m^{-3}, $\mathbf{v}$ is the velocity field in m·s^{-1}, P is the pressure field in Pa, and, finally, η is the viscosity in Pa·s. The fluid is assumed to be Newtonian, viscous, incompressible, and isothermal [39]. This last hypothesis is actually a consequence of the assumption of a uniform temperature in the defluoridator. As discussed previously in Section III-B1, the fluid is assumed to be dilute, therefore the electromagnetic forces on it can be neglected. To solve (14), at the inlet section, the velocity normal to the surface is set to $\mathbf{v}_0$. While, at the wall, represented by the metal plate and the plexiglass housing, the no slip condition applies [35], [50]

$$\mathbf{v} = 0. \tag{15}$$

The unknown velocity value at the outlets of the system in Fig. 2 is determined by imposing the pressure P to be equal to zero.

[1]Lenght at which the coulomb energy balances the thermal energy. At 20 °C, it is ∼7 Å. Therefore, the ion–ion statistical correlations can be neglected.

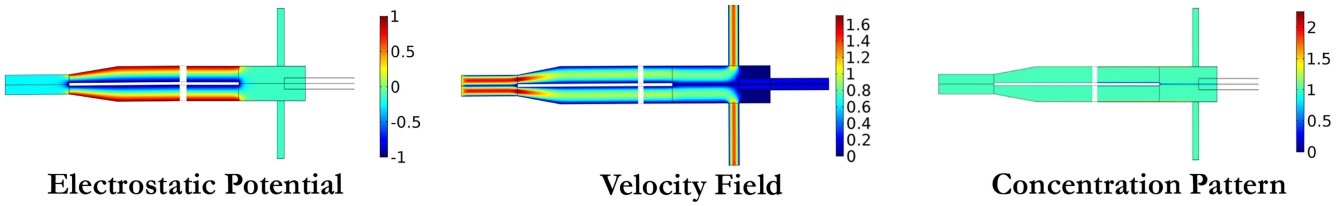

Fig. 6. Electrostatic potential ϕ distribution normalized to the applied voltage ϕ_0. Velocity field distribution normalized to the inlet velocity v_0. Concentration pattern normalized to the initial F^- concentration in the water.

Since the goal of the proposed electrostatic unit is to separate the charges contained in the fluid and then to collect them to different streams and outlets, the flow regime must be laminar to avoid mixing due to turbulence phenomena. A laminar fluid profile ensures the possibility to establish controllable and predictable concentration gradients. Therefore, the Reynolds number in the main body of the system is required to verify the following relationship for every v_0 value [39], [46]:

$$Re = \frac{\rho v_0 2 r_{\text{in}}}{\eta} \ll 5 \cdot 10^5 \tag{16}$$

where the characteristic length is set to the radius of the circular inlet section, r_{in} (for further details see Section SM7 of Supplementary material).

IV. Simulations Overview

Given the system presented in Section II and the mathematical framework described in Section III-B, it must be recognized that the parameter space of both the geometric and operative quantities is very large. Therefore, as explained better in Section SM3 in Supplementary material, in this article, the modeling of a complex and multiphysics dynamic system, such as electromigration, needs a careful analysis, which respects the assumptions of (10), (12), and (16). The system was studied assuming the existence of a steady-state solution for the mass transport equation and assuming the system to be weakly nonlinear for the following parameters:

1) $T \in (15\ ^\circ\text{C}; 45\ ^\circ\text{C})$;
2) $C_0 \in [10\ \text{mg}\cdot\text{L}^{-1}; 100\ \text{mg}\cdot\text{L}^{-1}]$;
3) $\text{v}_0 \in (1\ \text{mm}\cdot\text{s}^{-1}; 10\ \text{m}\cdot\text{s}^{-1}]$;
4) $\phi_0 \in [1\ \text{mV}; 2\ \text{V}]$.

The defluoridator was studied for the different working parameters in the ranges reported, by using the parameter given in Table ST1 from Supplementary Material. After having clarified and quantified the mutual influence of these quantities on the system performance, the channel length was varied to study if the probability of capturing the target F^- ion can be increased and the removal efficiency augmented [29]. The simulations were performed using the commercial FEM software COMSOL Multiphysics (COMSOL, Inc., Burlington MA, USA). In particular, the MPB equation (4) was solved using the *Mathematics* module while the drift-diffusion equation was implemented with the *Transport of Dilute Species* interface, and, finally, the Navier–Stokes equation (14) was calculated using the *Laminar Flow* interface. The fluidodynamic problem is first solved and the retrieved velocity field is inserted in the mass transport problem, coupled with the electrostatic one.

V. Results

The steady-state solution of the electric potential distribution, the velocity field $\mathbf{v}$, and the concentration patterns have been evaluated. The normalized results are presented in Fig. 6. Since the system in Fig. 2 has a very high aspect ratio, and since the solutions are constant for a considerable length, part of the main channel is not represented in order to favor the representation and understanding. From Fig. 6 it can be noticed that the electric field is constant between plates. Moreover, neither the electrostatic potential nor the electric field are affected by the water and charge flow. This is due to the fact that the velocity is null at the electrodes and plexiglass surface. As regards the water velocity, between the inner electrodes and the plastic tube, the profile has been verified to be perfectly parabolic. Finally, the salt concentration is constant in the bulk, whereas it sharply varies when approaching the charged surfaces. The configuration studied is the one with the inner electrodes set to the external voltage ϕ_0 while the inner metal plate is negatively charged. In this way, the surface available for the capture and transport of the ions is doubled. From Fig. 6, it can be observed that F^- ions are depleted near the inner metal plate while its density increases twofold at the positive electrode, thus implying that the target ion is highly concentrated at the outlets of the defluoridator system, demonstrating that the central stream can be easily collected.

The spatial dependence of the physical quantities ϵ, D, and μ, due to their explicit relationships with F^- concentration, was assessed along a cut-line, which starts from the surface of the inner electrode and goes to the surface of the plexiglass tube, in the x-direction, with $y = 50$ cm. The bulk was not depicted in Fig. 7 for the sake of representation. The F^- concentration profile follows the MPB distribution from (4), and the trend of the curves is in qualitative agreement with the results of [31] and [32]. Moving from the negatively charged surface, the target ion concentration increases to reach the bulk value C_0. Then, getting close to the positively charged electrodes, the gradient becomes steepen as the voltage increases, but the variable C_- augments and reaches a finite value, which is about two to six times the bulk concentration [see Fig. 7(a)]. This spatial distribution causes the dielectric permittivity to be higher nearby the inner plate, whereas it decreases at the plexiglass surface, according to the findings from [40], [45], and [51]. For low

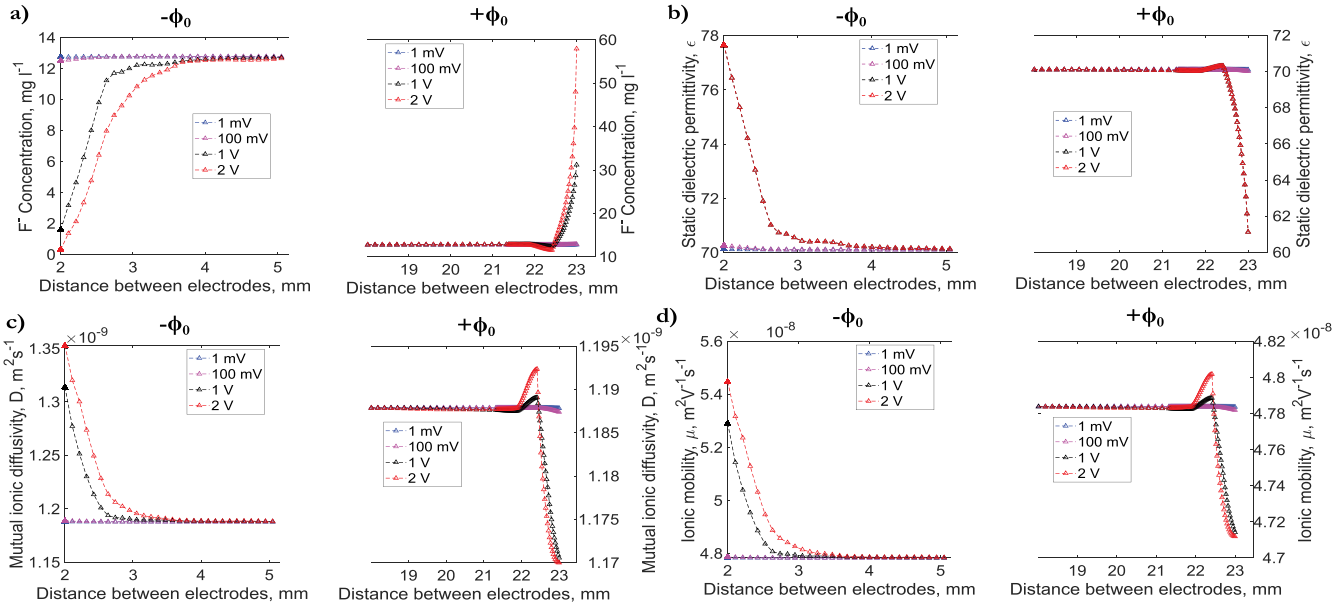

Fig. 7. (a) Fluoride concentration between the charged plates. (b) Dielectric permittivity between the electrodes. (c) Ionic diffusivity as a function of space and concentration. (d) Ionic mobility. The one-dimensional line corresponds to height $y = 50$ cm. The system temperature is 15 °C, and the inlet velocity is 1 mm·s^{-1}.

TABLE III
FLUORIDE REMOVAL (Γ, %) FOR DIFFERENT APPLIED VOLTAGES, WORKING TEMPERATURE, AND INITIAL ION CONCENTRATION

	C_0 = 10 mg·l^{-1}			C_0 = 50 mg·l^{-1}			C_0 = 100 mg·l^{-1}		
ϕ_0	T = 15°C	T = 30°C	T = 45°C	T = 15°C	T = 30°C	T = 45°C	T = 15°C	T = 30°C	T = 45°C
1 mV	0.161	0.157	0.154	0.160	0.157	0.154	0.160	0.157	0.154
100 mV	7.666	7.530	7.40	7.64	7.510	7.400	7.61	7.50	7.41
1 V	57.257	57.000	56.474	57.270	56.910	56.520	57.30	56.960	56.545
2 V	98.051	97.527	97.156	98.001	97.653	97.159	98.065	97.616	97.063

Inlet velocity is 0.1 m·s^{-1}.

voltages, the variation is negligible. While for high voltages (i.e., 1–2 V), as shown in Fig. 7(b), the permittivity varies significantly (∼21.79%) and hence it is possible to infer that it strongly influences the evaluated electrostatic potential, as well as the electric force on ions (4), (6). Therefore, the final concentration pattern affects the electrostatic potential distribution, which in turn strongly influences the ion spatial profile. However, the physical coupling is more complex. The presented mathematical framework accounts for such actual intricacy considering the ion diffusivity and ionic mobility to lower as the concentration increases [40]. As presented in Fig. 7(c) and (d), the transport properties of the F^- ion vary between the electrodes. In the repulsive region, D and μ are higher while reaching their minimum at the attraction surface (∼13.97% and 12.8% of variation). The temperature variation follows the trend described previously (data not shown). As regards the influence of the inlet velocity, between the plates, it was found a deviation of ∼0.05% between v_0 of 0.1 mm·s^{-1} and 10 cm·s^{-1}.

Considering the multiphysics coupling of electric and mass transport phenomena, it has been possible to evaluate the performance of the electrostatic, membraneless unit for the removal of fluoride from thermal waters under different operative conditions (see Section IV). The removal efficiency Γ was evaluated

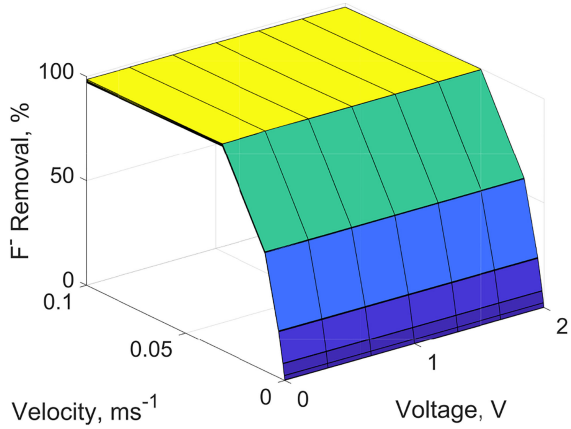

Fig. 8. Removal efficiency of fluoride ion, in %, versus applied voltage (ϕ_0, V) and inlet water velocity (v_0, m·s^{-1}). The working temperature is 15 °C and the initial F^- concentration is the lower bound value of 10 mg·L^{-1}.

as the average at the outlet sections of the collection channels (see Fig. 2). The results are reported in the surface plot of Fig. 8 and Table III. From Fig. 8, it can be noticed that the fluoride removal Γ is minimum when inlet velocities of about 1 mm·s^{-1}

are set, for any voltage value. On the other hand, as the water velocity increases, e.g., up to 0.1 m·s^{-1}, the effectiveness of the F^- removal increases, being maximum for high voltages. The difference between an applied voltage of 1 mV and 2 V is about 15%. The reciprocal influence of the other operative parameters, namely the initial concentration of fluoride C_0 and the system temperature T, was assessed. From Table III, it can be observed that the removal is almost constant (i.e., 1% variation, which is the precision limit of the numerical simulations) with the initial ion concentration C_0. However, the removal index Γ is a dimensionless number and it is normalized to C_0. Therefore, considering an applied voltage of 2 V, a working temperature of 15 °C, and a fluid velocity of 1 mm·s^{-1}, F^- collected at the outflows is 9.80 and 98.05 mg·ml^{-1} for Ethiopian thermal waters with 10 and 100 mg·mL^{-1} of F^-, respectively. Furthermore, from Table III, it can be noticed that the lower the temperature, the higher the fluoride removal. This is due to the fact that at 15 °C, the dielectric permittivity is lower [see Fig. 7(b)], implying a slightly stronger electric field, and to the lower diffusion coefficient of the ion [see Fig. 5 and 7(c)], which causes the electromigration and advection fluxes to be higher than the diffusion one. In mathematical terms, $\left|D\nabla C_-\right| < \left|-ze\mu C_-\nabla\phi + \mathbf{v}\nabla C_-\right|$. Despite the wider variations of ϵ, D, and μ presented in Fig. 3 and 5, a 30 °C temperature difference translates into a maximum variation of about 1% of Γ for the proposed electrostatic unit. In summary, from the numerical experiments, it has been found that the proposed electrostatic unit could work in moderate to high velocity regime, i.e., from 0.01 ms^{-1}, which implies a relatively high flow rate of water to be treated, and at high applied voltage, i.e., from 100 mV to 2 V. The proposed columnar electrostatic unit can properly treat the Ethiopian waters from Table II. Furthermore, it has been found that the working temperature of the system should be as low as possible. However, this parameter is not critical. This is a relevant finding since the temperature at water source may strongly vary among the Ethiopian sites [14], but the outcome of the defluoridation process varies by 1% across a 30 °C interval.

The last set of simulations was performed varying the length of the reactor to study the influence of this quantity on the system performance. The reactor was shrank to half its length and then enlarged up to three times the original size. The results are shown in Fig. 9. From Fig. 9, it can be noticed that when the length of the reactor is varied, the efficiency of fluoride removal strongly varies. This result indicates that also the geometric parameters can influence the system performances. For example, for an applied voltage of $\phi_0 = 1$ V, the defluoridation efficiency of the electrostatic unit drops from a maximum of 100%, for a length of 0.55 m, to 67.8% for a column 3.3 m long. The influence of the system length is more pronounced at lower voltages (e.g., 50 and 100 mV), then becoming almost not significant for low voltages (e.g., from 1 to 10 mV). The findings from Fig. 9 forecast future investigations and studies on whether an optima geometry exist for this type of membraneless defluoridation system.

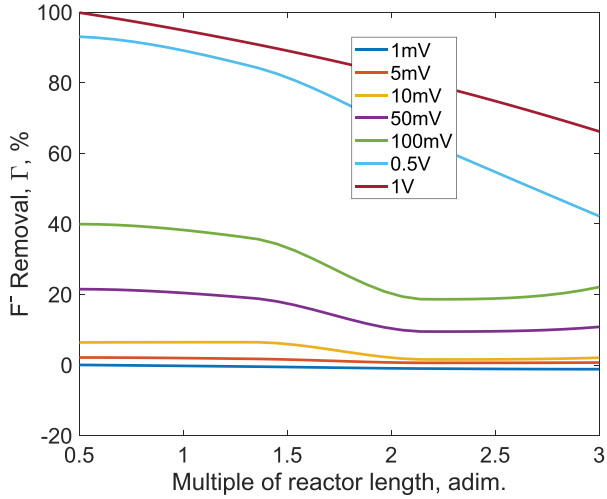

Fig. 9. Removal of fluoride ion for different length of the columnar reactor. The applied voltage has been varied from 1 mV to 1 V, whilst the working temperature was supposed to be 37 °C and the fluid velocity 0.1 ms^{-1}.

VI. Conclusion and Discussion

In this article, an electrostatic and membraneless unit for defluoridation of Ethiopian thermal waters was studied. This system applies a static electric field via parallel plates to separate the charges of a z:z binary and symmetric electrolyte (NaF) which is flowing in laminar regime. The problem was solved in the coupled Poisson–Nernst–Planck–Stokes scheme. The electromigration phenomenon was investigated for high salt concentration and strong applied voltages, assuming that the device can operate in condition of weakly nonlinear regime. The dielectric permittivity and both the ionic diffusivity and mobility have been considered to be a function of F^- concentration and of system temperature. This preliminary analysis allowed us to identify the values of applied voltages, input velocities, and Ethiopian water composition to be treated in order to satisfy water safety requirements [9].

Future works must deal with the problem of modeling the actual presence of multiple ions in the solution (see Table II). The system proposed therein, while reducing the fluoride ion presence, must not deprive water from essential constituents. Therefore, the nonlinear term in (6) must be completed considering each ionic contribution and interaction. Another point to be investigated is the possibility of employing an alternate current signal to elicit the movement of the ionic species [52]. This would introduce another free parameter, i.e., the frequency of the applied voltage, to the set of operating parameters. The possible electrosorption phenomenon at the inner electrode surface could be investigated relying on the model proposed by Yang *et al.* [53]. Finally, with the mathematical framework described in this article, the geometry of the system would be modified to identify different configurations of the electrodes or of the fluidic channels, and a suitable scaling to enhance the removal efficiency can be investigated.

ACKNOWLEDGMENT

The authors would like to gratefully thank B. Carasi, G. Rosati, and M. Torsello from COMSOL Multiphysics for their valuable help.

Finally, the authors are grateful to the anonymous reviewers for their valuable comments and constructive criticisms of the manuscript, which were very helpful to improve it.

REFERENCES

[1] Y. Qian, "Sustainable management of water resources," *Engineering*, vol. 2, no. 1, pp. 23–25, 2016.

[2] M. Mohapatra, S. Anand, B. K. Mishra, D. E. Giles, and P. Singh, "Review of fluoride removal from drinking water," *J. Environ. Manage.*, vol. 91, no. 1, pp. 67–77, 2009.

[3] M. Vithanage and P. Bhattacharya, "Fluoride in the environment: Sources, distribution and defluoridation," *Environ. Chem. Lett.*, vol. 13, no. 2, pp. 131–147, 2015.

[4] G. Biswas, M. Kumari, K. Adhikari, and S. Dutta, "A critical review on occurrence of fluoride and its removal through adsorption with an emphasis on natural minerals," *Current Pollut. Rep.*, vol. 3, no. 2, pp. 104–119, 2017.

[5] D. Cicchella *et al.*, "Trace elements and ions in italian bottled mineral waters: Identification of anomalous values and human health related effects," *J. Geochem. Exploration*, vol. 107, no. 3, pp. 336–349, 2010.

[6] E. Dinelli, A. Lima, B. De Vivo, S. Albanese, D. Cicchella, and P. Valera, "Hydrogeochemical analysis on Italian bottled mineral waters: Effects of geology," *J. Geochem. Exploration*, vol. 107, no. 3, pp. 317–335, 2010.

[7] M. S. McDonagh *et al.*, "Systematic review of water fluoridation," *BMJ*, vol. 321, no. 7265, pp. 855–859, 2000.

[8] Food and Agricultural Organization, "AQUASTAT—Main database," 2016. [Online]. Available: http://www.fao.org/nr/water/aquastat/data/query/index.html?lang=en

[9] World Health Organization, *Guidelines for Drinking-Water Quality*, vol. 1. Geneva, Switzerland: World Health Org., 2004.

[10] S. Peckham and N. Awofeso, "Water fluoridation: A critical review of the physiological effects of ingested fluoride as a public health intervention," *Sci. World J.*, vol. 2014, 2014, Art. no. 293019.

[11] L. S. Kaminsky, M. C. Mahoney, J. Leach, J. Melius, and M. Jo Miller, "Fluoride: Benefits and risks of exposure," *Crit. Rev. Oral Biol. Med.*, vol. 1, no. 4, pp. 261–281, 1990.

[12] P. T. Harrison, "Fluoride in water: A UK perspective," *J. Fluorine Chem.*, vol. 126, no. 11/12, pp. 1448–1456, 2005.

[13] M. Barathi, A. S. K. Kumar, and N. Rajesh, "Impact of fluoride in potable water—An outlook on the existing defluoridation strategies and the road ahead," *Coordination Chem. Rev.*, vol. 387, pp. 121–128, 2019.

[14] C. Reimann, K. Bjorvatn, B. Frengstad, Z. Melaku, R. Tekle-Haimanot, and U. Siewers, "Drinking water quality in the Ethiopian section of the East African Rift Valley I—Data and health aspects," *Sci. Total Environ.*, vol. 311, no. 1–3, pp. 65–80, 2003.

[15] A. Kumie and A. Ali, "An overview of environmental health status in Ethiopia with particular emphasis to its organization, drinking water and sanitation: A literature survey," *Ethiopian J. Health Develop.*, vol. 19, no. 2, pp. 89–103, 2005.

[16] Z. A. Alemu, K. T. Teklu, T. A. Alemayehu, K. H. Balcha, and S. D. Mengesha, "Physicochemical quality of drinking water sources in Ethiopia and its health impact: A retrospective study," *Environ. Syst. Res.*, vol. 4, no. 1, 2015, Art. no. 22.

[17] L. Osterwalder, C. A. Johnson, H. Yang, and R. B. Johnston, "Multi-criteria assessment of community-based fluoride-removal technologies for rural Ethiopia," *Sci. Total Environ.*, vol. 488, pp. 532–538, 2014.

[18] S. Jagtap, M. K. Yenkie, N. Labhsetwar, and S. Rayalu, "Fluoride in drinking water and defluoridation of water," *Chem. Rev.*, vol. 112, no. 4, pp. 2454–2466, 2012.

[19] P. Loganathan, S. Vigneswaran, J. Kandasamy, and R. Naidu, "Defluoridation of drinking water using adsorption processes," *J. Hazardous Mater.*, vol. 248, pp. 1–19, 2013.

[20] M. Errico, F. Desogus, M. Mascia, G. Tola, and L. Dendena, "Soil adsorption defluoridation of drinking water for an Ethiopian rural community," *Chem. Papers*, vol. 60, no. 6, pp. 460–465, 2006.

[21] A. B. Nasr, K. Walha, C. Charcosset, and R. B. Amar, "Removal of fluoride ions using cuttlefish bones," *J. Fluorine Chem.*, vol. 132, no. 1, pp. 57–62, 2011.

[22] Z. Amor, B. Bariou, N. Mameri, M. Taky, S. Nicolas, and A. Elmidaoui, "Fluoride removal from brackish water by electrodialysis," *Desalination*, vol. 133, no. 3, pp. 215–223, 2001.

[23] L. J. Banasiak, T. W. Kruttschnitt, and A. I. Schäfer, "Desalination using electrodialysis as a function of voltage and salt concentration," *Desalination*, vol. 205, no. 1–3, pp. 38–46, 2007.

[24] M. Arda, E. Orhan, O. Arar, M. Yuksel, and N. Kabay, "Removal of fluoride from geothermal water by electrodialysis (ED)," *Sep. Sci. Technol.*, vol. 44, no. 4, pp. 841–853, 2009.

[25] S. Lahnid *et al.*, "Economic evaluation of fluoride removal by electrodialysis," *Desalination*, vol. 230, no. 1–3, pp. 213–219, 2008.

[26] J. Zhu, H. Zhao, and J. Ni, "Fluoride distribution in electrocoagulation defluoridation process," *Sep. Purifi. Technol.*, vol. 56, no. 2, pp. 184–191, 2007.

[27] J. Padmasiri and C. Dissanayake, "A simple defluoridator for removing excess fluorides from fluoride-rich drinking water," *Int. J. Environ. Health Res.*, vol. 5, no. 2, pp. 153–160, 1995.

[28] W.-H. Choi, J.-W. Shin, J.-J. Kim, and J.-Y. Park, "Calcite-packed columns for the removal of fluoride in industrial wastewater," *Desalin. Water Treat.*, vol. 30, no. 1–3, pp. 247–253, 2011.

[29] F. Alnaimat, E. Alhseinat, F. Banat, and V. Mittal, "Electromagnetic–mechanical desalination: Mathematical modeling," *Desalination*, vol. 380, pp. 75–84, 2016.

[30] R. Tekle-Haimanot *et al.*, "The geographic distribution of fluoride in surface and groundwater in Ethiopia with an emphasis on the rift valley," *Sci. Total Environ.*, vol. 367, no. 1, pp. 182–190, 2006.

[31] M. S. Kilic, M. Z. Bazant, and A. Ajdari, "Steric effects in the dynamics of electrolytes at large applied voltages. I. Double-layer charging," *Phys. Rev. E*, vol. 75, no. 2, 2007, Art. no. 021502.

[32] M. S. Kilic, M. Z. Bazant, and A. Ajdari, "Steric effects in the dynamics of electrolytes at large applied voltages. II. Modified Poisson–Nernst–Planck equations," *Phys. Rev. E*, vol. 75, no. 2, 2007, Art. no. 021503.

[33] I. Borukhov, D. Andelman, and H. Orland, "Adsorption of large ions from an electrolyte solution: A modified Poisson–Boltzmann equation," *Electrochimica Acta*, vol. 46, no. 2/3, pp. 221–229, 2000.

[34] P. Attard, "Electrolytes and the electric double layer," *Adv. Chem. Phys.*, vol. 92, pp. 1–160, 1996.

[35] J. Lu, D.-J. Li, L.-L. Zhang, and Y.-X. Wang, "Numerical simulation of salt water electrolysis in parallel-plate electrode channel under forced convection," *Electrochimica Acta*, vol. 53, no. 2, pp. 768–776, 2007.

[36] G. Bauer, V. Gravemeier, and W. A. Wall, "A 3D finite element approach for the coupled numerical simulation of electrochemical systems and fluid flow," *Int. J. Numer. Methods Eng.*, vol. 86, no. 11, pp. 1339–1359, 2011.

[37] M. Burger, B. Schlake, and M.-T. Wolfram, "Nonlinear Poisson–Nernst–Planck equations for ion flux through confined geometries," *Nonlinearity*, vol. 25, no. 4, pp. 961–990, 2012.

[38] Y. Sun, P. Sun, B. Zheng, and G. Lin, "Error analysis of finite element method for Poisson–Nernst–Planck equations," *J. Comput. Appl. Math.*, vol. 301, pp. 28–43, 2016.

[39] M. Schmuck, "Analysis of the Navier–Stokes–Nernst–Planck–Poisson system," *Math. Models Methods Appl. Sci.*, vol. 19, no. 6, pp. 993–1014, 2009.

[40] R. Lu and D. G. Leaist, "Mutual diffusion in solutions of alkali metal halides aqueous LiF, NaF and KF at 25 °C," *J. Chem. Soc., Faraday Trans.*, vol. 94, no. 1, pp. 111–114, 1998.

[41] R. Buchner, G. T. Hefter, and J. Barthel, "Dielectric relaxation of aqueous NaF and KF solutions," *J. Chem. Soc., Faraday Trans.*, vol. 90, no. 17, pp. 2475–2479, 1994.

[42] P. S. Ray, "Broadband complex refractive indices of ice and water," *Appl. Opt.*, vol. 11, no. 8, pp. 1836–1844, 1972.

[43] A. Fanti, M. Spanu, M. B. Lodi, F. Desogus, and G. Mazzarella, "Nonlinear analysis of soil microwave heating: Application to agricultural soils disinfection," *IEEE J. Multiscale Multiphys. Comput. Techn.*, vol. 2, pp. 105–114, 2017.

[44] F. Booth, "The dielectric constant of water and the saturation effect," *J. Chem. Phys.*, vol. 19, no. 4, pp. 391–394, 1951.

[45] E. Gongadze, U. van Rienen, V. Kralj-Iglič, and A. Iglič, "Langevin Poisson–Boltzmann equation: Point-like ions and water dipoles near a charged surface," *General Physiol. Biophys.*, vol. 30, no. 2, pp. 130–137, 2011.

[46] E. L. Cussler, *Diffusion: Mass Transfer in Fluid Systems*. Cambridge, U.K.: Cambridge Univ. Press, 2009.

[47] S. H. Lee and J. C. Rasaiah, "Molecular dynamics simulation of ionic mobility. I. Alkali metal cations in water at 25 °C," *J. Chem. Phys.*, vol. 101, no. 8, pp. 6964–6974, 1994.

[48] S. H. Lee and J. C. Rasaiah, "Molecular dynamics simulation of ion mobility. 2. Alkali metal and halide ions using the SPC/E model for water at 25 °C," *J. Phys. Chem.*, vol. 100, no. 4, pp. 1420–1425, 1996.
[49] B. J. Kirby, *Micro-and Nanoscale Fluid Mechanics: Transport in Microfluidic Devices*. Cambridge, U.K.: Cambridge Univ. Press, 2010.
[50] E. Lauga, M. P. Brenner, and H. A. Stone, "The no-slip boundary condition: A review," 2005, *arXiv:0501557*.
[51] P. Marracino, M. Liberti, G. d'Inzeo, and F. Apollonio, "Water response to intense electric fields: A molecular dynamics study," *Bioelectromagnetics*, vol. 36, no. 5, pp. 377–385, 2015.
[52] L. H. Olesen, M. Z. Bazant, and H. Bruus, "Strongly nonlinear dynamics of electrolytes in large ac voltages," *Phys. Rev. E*, vol. 82, no. 1, 2010, Art. no. 011501.
[53] K.-L. Yang, T.-Y. Ying, S. Yiacoumi, C. Tsouris, and E. S. Vittoratos, "Electrosorption of ions from aqueous solutions by carbon aerogel: An electrical double-layer model," *Langmuir*, vol. 17, no. 6, pp. 1961–1969, 2001.

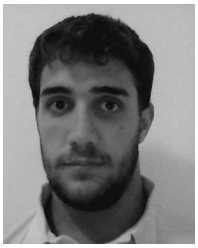

Matteo Bruno Lodi (Student Member, IEEE) was born in Cagliari, Italy, on January 15, 1994. He received the bachelor's degree from the University of Cagliari, Cagliari, Italy, in 2016, and the master's degree from the Politecnico di Torino, Torino, Italy, in 2018, both in biomedical engineering. He is currently working toward the Ph.D. degree in electronic engineering and computer science with the University of Cagliari.

His current research interests activity deals with the modeling of bioelectromagnetic phenomena, the study, manufacturing, and synthesis of magnetic biomaterials for tissue engineering applications, and the use of microwave for biotechnology and environmental applications.

Fabio Fanari was born in Oristano, Italy, on August 18, 1991. He received the bachelor's degree in chemical engineering and the master's degree in chemical engineering and biotechnological processes from the University of Cagliari, Cagliari, Italy, in 2014 and 2017, respectively. He is currently working toward the Ph.D. degree in industrial engineering with the University of Cagliari.

His current research activity mainly deals with the food process engineering and the materials characterization, especially using rheological measurements and dielectric spectroscopy.

Alessandro Fanti (Member, IEEE) received the Laurea degree in electronic engineering and the Ph.D. degree in electronic engineering and computer science from the University of Cagliari, Cagliari, Italy, in 2006 and 2012, respectively.

From 2013 to 2016, he was a Postdoctoral Fellow with the Electromagnetic Group, University of Cagliari, where he is currently an Assistant Professor. His current research interests involves the use of numerical techniques for modes computation of guiding structures, optimization techniques, analysis and design of waveguide slot arrays, analysis and design of patch antennas, radio propagation in urban environment, modeling of electromagnetic phenomena, microwave exposure systems for biotechnology, and bioagriculture.

Francesco Desogus received the master's (with honors) degree in chemical engineering and the Ph.D. degree in industrial engineering from the University of Cagliari, Cagliari, Italy, in 2005 and 2010, respectively.

Since 2014, he has been an Assistant Professor with the Department of Mechanical, Chemical and Materials Engineering, University of Cagliari. He taught courses of organic chemistry, industrial and energy processes, and chemical plants, and currently is a Lecturer in transport phenomena for environment protection. His current research interests include chemical and biological kinetics, chemical reactors, transport phenomena, and biomass processing.

Worash Getaneh received the B.Sc. and M.Sc. degrees in geology from Addis Ababa University, Addis Ababa, Ethiopia, in 1990 and 1993 respectively, and the Ph.D. degree in geoengineering from the University of Cagliari, Cagliari, Italy in 1999.

He is currently an Associate Professor in geology with the School of Earth Sciences, Addis Ababa University. His current research interest is in the broad fields of mineral deposits, mining geology, geochemistry, and environmental geology.

Dr. Getaneh is a Member of the Ethiopian Geosciences and Mineral Engineering Association, Geological Society of Africa, and International Association of Impact Assessment.

Giuseppe Mazzarella (Senior Member, IEEE) received the graduate degree (*summa with laude*) in electronic engineering from the Università Federico II of Naples, Naples, Italy, in 1984, and the Ph.D. degree in electronic engineering and computer science in 1989 from the Università Federico II of Naples, Nepales.

In 1990, he became an Assistant Professor with the Dipartimento di Ingegneria Elettronica, Università Federico II of Naples. Since 1992, he has been with the Dipartimento di Ingegneria Elettrica ed Elettronica, Università di Cagliari, Cagliari, Italy, first as an Associate Professor and then, since 2000, as a Full Professor, teaching courses in electromagnetics, microwave, antennas, and remote sensing. He is an author or coauthor of more than 70 papers in international journals, and is a Reviewer for many electromagnetic journals. His current research activity has focused mainly on efficient design of large arrays of slots, power synthesis of array factor, with emphasis on inclusion of constraints, microwave holography techniques for the diagnosis of large reflector antennas, and use of evolutionary programming for the solution of inverse problems, in particular problems of synthesis of antennas and periodic structures.

Paolo Valera received the graduate degree in geology from the University of Cagliari, Cagliari, Italy, in 1996, and the Ph.D. degree from University of Trieste, Trieste, Italy, in 2000.

His fieldwork for graduate and Ph.D. degrees was carried out in Ethiopia. He became an Associate Professor with the University of Cagliari in 2019. In February 2008, he has been involved in the geochemical mapping of agricultural and grazing soils of Europe and the European Ground Water Geochemistry projects, as local P.I. Associated to National Research Council (CNR). In 2009, he founded the Associazione Italiana di Geologia Medica (Italian Medical Geology Association).

Dr. Valera is a Member of International Union of Geological Sciences Commission on "Global Geochemical Baselines." He was a Coordinator of International Agreement Between the University of Cagliari and the University of Addis Ababa from 2011 to 2016 and of a Memorandum of Understanding between the University of Cagliari and the Universitat de Lleida from 2013 to 2018. He is an author of more than 30 international peer-reviewed publications and more of 180 various scientific products.